ACADEMIC PRESS

Method for functional MRI mapping of nonlinear response

Peter Kellman,[a,]* Peter van Gelderen,[b] Jacco A. de Zwart,[b] and Jozef H. Duyn[b]

[a] *Laboratory of Cardiac Energetics, NHLBI, National Institutes of Health, Bethesda, MD 20892 USA*
[b] *Advanced MRI, Laboratory of Functional and Molecular Imaging, NINDS, National Institutes of Health, Bethesda, MD 20892 USA*

Abstract

Nonlinear systems analysis combining blood oxygen level dependent (BOLD), functional magnetic resonance imaging (fMRI) and m-sequence stimulation paradigms are proposed as a new method for exploring neuronal responses and interactions. Previous studies of electrical activity in the human visual cortex have observed significant nonlinearities of task-induced activity with temporal dynamics on a timescale of 10–20 ms. Despite the confounding effect of the seconds-long hemodynamic response, it is demonstrated that BOLD fMRI can be used to probe neuronal interactions on a time scale of tens of ms. Visual activation experiments were performed with various stimuli, and amplitude maps of first and second order kernel coefficients were generated using correlation analysis. Second order nonlinearities in BOLD fMRI were observed and attributed to temporal contrast caused by transitions in the stimulus sequence. In addition, the kernel maps showed significant differences between second order nonlinearities of foveal and peripheral vision. By including a reference experiment with a slightly modified stimulus presentation, a distinction could be made between (fast) neuronal nonlinearities and hemodynamic effects on the time scale of the seconds. The results indicate that BOLD fMRI can probe fast neuronal nonlinearities.

Introduction

Nonlinear systems analysis of brain function provides valuable information about neuronal processes and interaction. Electrical recordings have been used to analyze various brain functions, with a large number focusing on the visual system. Substantial nonlinear effects have been noted along the visual pathway, including retina, lateral geniculate nucleus (LGN), and cortex. Although electrical recordings can provide exquisite temporal information of spiking processes and development of local field potentials, they are either invasive or have limited spatial resolution. Functional magnetic resonance imaging (fMRI) based on blood oxygen level dependent (BOLD) contrast has excellent spatial resolution, but its temporal resolution is compromised by the substantial blurring and it has potential nonlinearities caused by the vascular effects that are responsible for its contrast mechanism. However, despite these limitations, a recent study has suggested that BOLD fMRI can be used to study specific neuronal interactions (Ogawa et al., 2000). The temporal resolution of BOLD fMRI is thought to be primarily limited by the slow hemodynamic response to neuronal processes. In order to estimate the hemodynamic response function, a number of authors have investigated the temporal dynamics of the fMRI signal in response to neuronal stimulation. Several research groups have investigated linearity of the fMRI BOLD response (Ogawa et al., 2000; Boynton et al., 1996; Glover, 1999; Vazquez and Noll, 1998; Friston et al., 1998; Birn et al., 2001). The principle of linear superposition has been tested (Boynton et al., 1996; Vazquez and Noll, 1998) by varying the stimulus duration and amplitude, and deviations from linearity were observed. The cause of the nonlinear fMRI response has been hypothesized (Friston et al., 2000) to be due to blood flow and BOLD effect based on a balloon model (Buxton et al., 1998). The primary motivation for estimating the hemodynamic response function has been for optimizing the detection of fMRI BOLD activation. In practice, the simplifying assumption of linear superposition is often used (Boynton et al., 1996; Bandettini et al., 1993; Friston et al., 1994).

* Corresponding author. National Institutes of Health, NHLBI, 10B1D416, 10 Center Drive, Bethesda, MD 20892. Fax: +1-301-402-2389.

E-mail address: kellman@nih.gov (P. Kellman).

In order to characterize nonlinear systems, Volterra–Wiener functional expansions may be used to model the system by analyzing the system response to appropriate input stimuli. The Volterra and Wiener models have been applied to several areas. For example, Marmarelis and Marmarelis (1978) applied the Wiener theory to modeling and identification of biological systems. Friston et al. (1998) characterized the BOLD response using a Volterra kernel model, and estimated first and second order kernels of a truncated second order model using a basis fitting approach. Basis fitting enforces a model that may result in an incorrect kernel estimate. The approach taken here using correlation analysis does not require basis fitting. A comprehensive description on the Volterra and Wiener theories of nonlinear systems is given by Schetzen (1980) and a concise survey and history of nonlinear system identification methods is presented by Billings (1980).

Nonlinear systems analysis using m-sequence probe stimuli was described by Sutter (1987). The m-sequence method offers practical benefits of ease of implementation as well as reduced statistical fluctuation as compared to white Gaussian noise probes. Application of m-sequence probing has been described for measuring the second order nonlinear neuronal response of the visual system using electrode recordings (Benardete and Kaplan, 1997; Reid et al., 1997; Baseler and Sutter, 1997; Sutter, 2001). Benardete and Victor (1994) describe an extension of the m-sequence technique for multi-input systems analysis.

Here, we propose the application of the m-sequence probing method to produce fMRI maps of the first and second order responses for several visual stimuli. The measured fMRI BOLD response to the visual stimulus is the result of a cascade of neuronal responses from the retina, LGN, and cortex, as well as the hemodynamic and BOLD effect (Buxton et al., 1998; Miller et al., 2001). It will be shown that, by including a reference experiment with a slightly modified stimulus presentation, the method allows distinction between (fast) neuronal nonlinearities and effects on the time scale of the seconds-long BOLD response. The observed second order response disappeared by introducing a decorrelating delay between m-sequence stimuli which was larger in duration than presumed neuronal response (tens of ms) but smaller than the BOLD effect (several seconds). Based on the assumption that the temporal dynamics of the neuronal system are much faster than the hemodynamic effects, these tests indicate that the second order response was predominately neuronal related corresponding to transitions in the stimulus sequence.

Methods

Nonlinear systems identification

The Volterra and Wiener models of nonlinear systems with memory can be used to analyze systems without as-

suming a known internal structure. The Volterra series expansion of the system output, $y(t)$, in response to an input $x(t)$ may be written as

$$
y(t) = k_0 + \sum_{n=0}^{T} k_1(n) x(t-n) +
$$
$$
\sum_{n_1=0}^{T} \sum_{n_2=0}^{T} k_2(n_1, n_2) x(t-n_1) x(t-n_2) +
$$
$$
\sum_{n_1=0}^{T} \sum_{n_2=0}^{T} \sum_{n_3=0}^{T} k_3(n_1, n_2, n_3) x(t-n_1) x(t-n_2) x(t-n_3)
$$
$$
+ \dots, \tag{1}
$$

with Volterra functionals defined by multidimensional convolutions with Volterra kernels $k_i (n_1, n_2, \dots n_i)$, and T as the system memory. Wiener (1958) proposed an orthogonalization procedure for the Volterra functionals using white Gaussian noise as the input stimulus. The Wiener model is an orthonormal expansion obtained by applying the Gram–Schmidt procedure to the Volterra functional representation,

$$
y(t) = [h_0] + \left[\sum_{n=0}^{T} h_1(n) x(t-n) \right]
$$
$$
+ \left[\sum_{n_1=0}^{T} \sum_{n_2=0}^{T} h_2(n_1, n_2) x(t-n_1) x(t-n_2) \right.
$$
$$
\left. - \sigma^2 \sum_{n=0}^{T} h_2(n, n) \right] + \dots, \tag{2}
$$

where the Wiener functionals (bracketed expressions) are orthogonal and σ^2 is the noise power assuming white Gaussian noise input, $x(t)$. Based on Wiener's results, Lee and Schetzen (1965) developed a practical cross-correlation method for measuring Wiener kernels with white Gaussian noise input, $x(t)$. The first several Wiener kernels, h_n, may be measured by the correlation method as

$$
h_0 = \langle y(t) \rangle
$$
$$
h_1(n) = \langle y(t) x(t-n) \rangle
$$
$$
h_2(n_1, n_2) = \frac{1}{2!} \langle y(t) x(t-n_1) x(t-n_2) \rangle, \text{ for } n_1 \neq n_2.
$$
$$
\tag{3}
$$

Note that if the actual system is indeed second order, i.e., Volterra kernels are zero for higher orders, then the Volterra and Wiener kernels are the same, with the exception of the diagonal terms. However, for higher order systems, truncated second order Volterra and Wiener models are different.
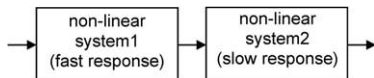
Fig. 1. Simplified model of cascade of nonlinear systems, each comprised of various sources (feedback mechanisms not shown).

M-sequence probes may be used instead of white Gaussian noise to reduce statistical fluctuation in the kernel estimate. The use of m-sequence probes has been described by Sutter, and a mathematical treatment has been presented by Benardete and Victor (1994) that includes the anomalous correlations that result due to the algebraic structure of the m-sequences. By replacing the white Gaussian noise probe by an m-sequence and integrating over a full period, the resultant estimates contain a small bias, order of $1/P$ where P is the period of the sequence, plus anomalous contributions which arise as a consequence of the fact that the true system is higher order than the model, and that the m-sequence probe has higher order auto-correlations. The bias is generally negligible for reasonable length sequences. The anomalous correlations may be largely mitigated by using the inverse repeat method and by judicious choice of m-sequence. The inverse repeat method consists of measuring the system response to both the m-sequence and its inverse (inverting polarity of bits). In this way, the odd and even order responses may be separated by calculating the sum and difference of the m-sequence correlations, respectively. For nonlinear systems with a small number of non-zero kernel coefficients, it is often possible to choose a sequence which will separate the remaining desired terms (described later). This was the approach used in this work. Benardete and Victor (1994) propose a hybrid m-sequence method in order to further mitigate anomalies, if required, based on a probe consisting of sums of m-sequences (multilevel sequence).

Cascade system

Nonlinear systems identification by a functional expansion, as described above, produces a nonparametric representation ("black box"), as opposed to a block structured approach based on a system model. The measured fMRI BOLD response to visual stimuli is actually a cascade system which includes the complete retinocortical path as well as neurovascular, and hemodynamic responses and their effect on blood oxygenation and MRI signal strength. The identification of structured models of nonlinear cascade systems is very complex, if indeed possible, and is not proposed here. Nevertheless, it is of interest to discriminate, if possible, whether the second order response in the fMRI BOLD measurement is caused by nonlinearities which are neuronal in origin or due to the hemodynamic response. The neurovascular mechanisms may contain fast as well as slow components. The neuronal response is characteristically fast with response time on the order of tens of ms, whereas the hemodynamic contribution to the measured BOLD response is several seconds in duration. A simplified model shown in Fig. 1 separates the fast and slow responses, ignoring feedback responses such as adaption of the pupil or cortical input to the LGN. Such a cascade model suggests that probe measurements may possibly be designed to discriminate fast and slow responses. This was examined by repeated measurement of the second order response after introducing a small delay or gap each period between the presentation of stimuli which were controlled by the m-sequence bits. The gap served to decorrelate the measured second order response (i.e., correlation with transitions). A uniform gray stimulus with zero contrast was presented during the gap.

Consider each nonlinear system to be a simple Wiener model (LN) consisting of a cascade of dynamic linear system (L_1) with memory and a static, memoryless nonlinearity (N_1). Fig. 2 shows the inputs and outputs of the hypothetical L_1N_1 model for various experimental paradigms (details
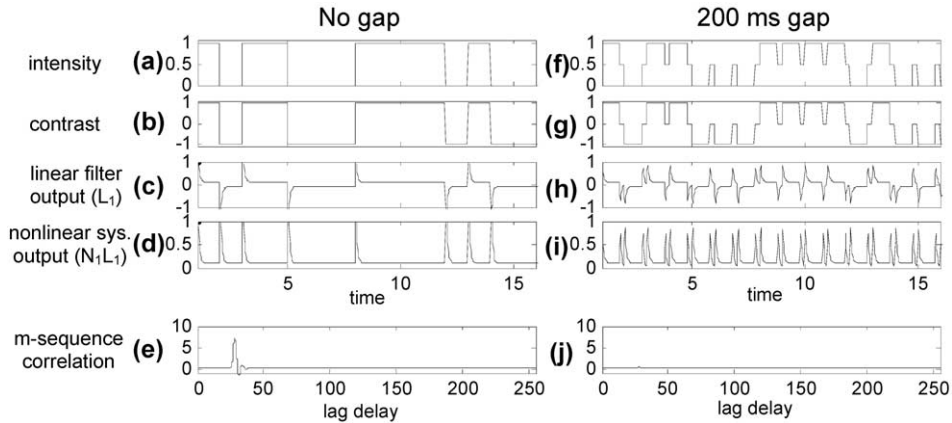

Fig. 2. Simulated waveforms for bullseye-reversal paradigm without gap (a–e) and with a 200-ms gap (f–j) illustrating: (a,f) input intensity; (b,g) signed (spatial) contrast; (c,h) linear filter (L_1) output; (d,i) rectified (L_1N_1) output; and (e,j) m-sequence correlation with output of nonlinear cascade ($L_1N_1L_2N_2$) system model.
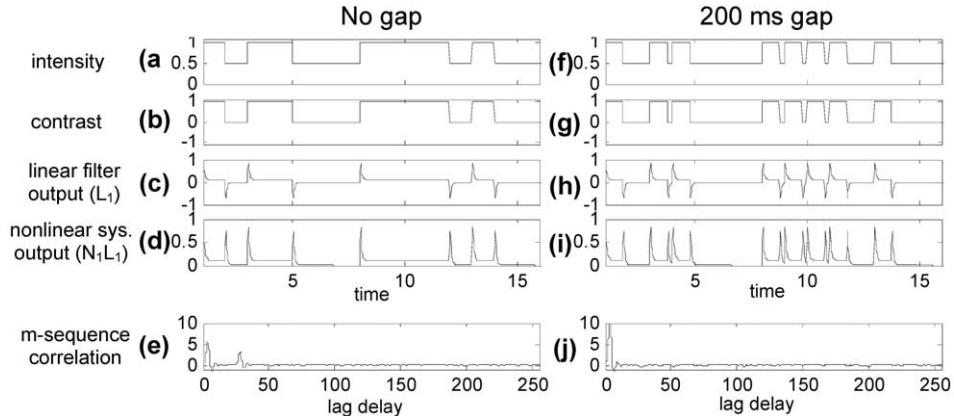
Fig. 3. Simulated waveforms for bullseye-gray paradigm without gap (a–e) and with a 200-ms gap (f–j) illustrating: (a,f) input intensity; (b,g) signed (spatial) contrast; (c,h) linear filter (L_1) output; (d,i) rectified (L_1N_1) output; and (e,j) m-sequence correlation with output of nonlinear cascade ($L_1N_1L_2N_2$) system model.

below) to illustrate the effect of a small decorrelating delay (gap). Figs. 2a–e correspond to a bullseye-reversal paradigm without a gap and Figs. 2f–j have a 200-ms gap. The inputs (Fig. 2a) are the image intensity for the first 16 bits of the m-sequence, where values 0, 1/2, and 1 correspond to black, gray, and white, respectively, and the intensity is for a check that is initially white. The spatial contrast is plotted in Fig. 2b, calculated at the edges between black and white. It is assumed that the signed contrast is input to a bandpass linear filter (L_1) followed by nonlinear rectification (N_1). The filter has an attenuated DC response which determines the sensitivity to constant luminance. The linear filter output is shown in Fig. 2c and rectified output in Fig. 2d. The L_1N_1 output shown in Fig. 2d consists of spikes at the m-sequence bit transitions giving rise to a second order kernel $h_2(i,i\text{-}1)$ (off-diagonal), whereas, by introducing a delay which is longer than the filter response duration, the output, Fig. 2i, consists of a constant train of spikes which is uncorrelated with the sequence or transitions. The resultant output of a cascade of fast and slow nonlinear dynamic systems was simulated using a $L_1N_1L_2N_2$ sandwich model, where L_1N_1 corresponds to the fast neuronal system described above, and L_2N_2 corresponds to the much slower hemodynamic response. Plots of the full-period m-sequence correlation with the $L_1N_1L_2N_2$ cascade output are shown in Figs. 2e and j corresponding to no gap and 200-ms gap, respectively. The L_2N_2 model used a lowpass filter (L_2) with 3.5-s half-width response followed by rectification (N_2). Note that the bullseye-reversal paradigm has no linear kernel response in this model, since the bipolar signed contrast signal proportional to the m-sequence is constant after rectification. Using a gap which is shorter than the linear filter response duration would not decorrelate the second order response.

Using a bullseye-gray experimental paradigm results in a linear kernel response both with and without a delay (gap) since the proportional signal (DC response) is unipolar, and contains a proportional signal after rectification. Fig. 3 shows a simulation of the $L_1N_1L_2N_2$ model system for the

bullseye-gray stimulus paradigm, with and without gap. The results and interpretation of these experiments will be described later. The results would be similar using a slightly more complicated sandwich model (LNL).

Stimulus timing

The binary m-sequence 0's and 1's were used to select between visual stimuli for the various experimental paradigms. The m-sequence was extended to include a portion of the next period to enable discarding of the initial transient. The extended m-sequence was then inverted and repeated. Using a 255-length m-sequence, the extended sequence was 300 bits, which yielded a total of 600 bits for the length of the run with the inverse repeat, corresponding to a 10-min duration scan at 1 s repetition per volume. For specific experiments, a small (variable) gap (e.g., 200 ms) was introduced between bits during which the visual stimulus was switched to gray. In this case, the bullseye would appear for 800 ms followed by 200 ms gray.

Block paradigms were used to produce t-score maps of the fovea and periphery regions. Block paradigms repeatedly alternated between 30 s fovea bullseye reversals and 30 s bullseye annulus reversals for a total of 300 s (images described below).

Binary m-sequence selection

The binary m-sequence used was selected such that the second order responses resulting from the first several second order kernel coefficients would not overlap with the linear response. In order to ensure that second order kernel responses $h_2(i,i\text{–}j)$ at the first several lag delays ($j = 1,2,3,...$) have adequate delay separation, the following design criterion was used. The linear kernel (hemodynamic response function) has a several seconds width (full width half maximum) but is followed by a lengthy undershoot. The total response duration was estimated to be approxi-
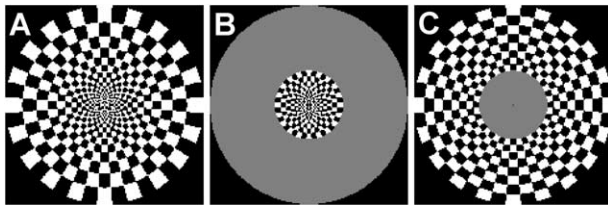
Fig. 4. Visual stimulus images used in various experimental paradigms: (A) bullseye; (B) foveal bullseye; and (C) peripheral annulus.

mately 20 s. It was desired to maximally separate the second order responses for at least the first 5 lag delays, where each lag corresponds to the m-sequence bit period = 1 s (imaging frame repetition). Using the shift and add property of the m-sequence (Golomb, 1968), i.e., $a_{i-k} = a_i \oplus a_{i-j}$ where $\oplus$ denotes a mod 2 sum, a binary m-sequence was chosen with period $2^8 - 1 = 255$ (generated by a linear feedback shift register with taps at 4, 5, 6, and 8) and was computed to have a minimum separation of 24 bits (s) for the first 6 lag delays, which occur at $j = 25, 49, 221, 97, 134$, and 186. In this way, the off-diagonal slices of the second order kernel $h_2(i,i-j) = r_{xy}(i-j)$ ($i = 1, 2, \ldots 20$ and $j = 1, 2, \ldots 5$) will be separated, where r_{xy} is the full-period m-sequence correlation. Tests were conducted using other m-sequences and the second order correlations were detected at other delay lags as predicted (not shown).

Visual stimuli

The visual stimuli were displayed using the Presentation software application (Neurobehavioral Systems, Inc.) running on a PC, which was triggered once per second by the MR scanner to synchronize the stimulus with data acquisition. An LCD projector (Sharp Notevision6) with long throw lens was used to project the images onto a screen directly in front of the magnet bore. Maximum luminance varied between 85 and 105 cd/m^2, as measured with a Minolta LS100 luminance meter with the projection screen set up outside the magnet. The image intensity reached 90% of the on or off value within 10 ms of a change, as measured with a photodiode. Bullseye images were black and white (100% contrast) with check size scaled with eccentricity (see Fig. 4A) in an attempt to maintain a constant stimulation across the area of primary visual cortex (i.e., constant spatial frequency across the receptive field) (Horton and Hoyt, 1991). The full bullseye spanned an eccentricity of approximately 8.2° and had a small central spot that alternated slowly between two colors as a fixation task. Various paradigms included: (1) bullseye and reverse, (2) bullseye and uniform gray, (3) uniform black and white disk, and (4) bullseye (2.5° eccentricity corresponding to foveal region) and bullseye annulus (2.5–8.2° periphery excluding fovea). The foveal and peripheral annulus bullseyes are shown in Figs. 4b and c, respectively. In paradigms 1–3 a uniform gray image was used in cases which used a gap between bits

of the m-sequence. The gray level was set to maintain a constant luminance, i.e., midway between black and white after gamma correction. The gamma correction was important to minimize flicker due to scattered light.

Imaging parameters

Imaging was performed on a GE 3T LX scanner using various head coils. A single-shot echo-planar imaging sequence was used with the following parameters: TE = 40 ms, TR = 1 s, 70° RF flip angle, ramp sampled with 23 ms acquisition window, and 8 slices acquired each TR. The acquisition matrix was 64 × 48 with typically 24 cm FOV (3/4 phase FOV) producing a nominal resolution of 3.75 × 3.75 mm^2 and 4 mm slice thickness. A bipolar gradient crusher was used to reduce contribution from large vessels. The image plane orientation was parallel to the calcarine fissure, with the volume containing the V1 cortical region. The initial image in each scan provided a low-resolution T2*-weighted anatomical reference. In addition, high-resolution anatomical scans were performed as well. All individuals in this study were normal, healthy volunteers giving informed consent. This study was performed in accordance with an NIH-approved protocol, reviewed by the NINDS IRB.

Processing and analysis

Raw data were acquired by the scanner and all processing was performed in software. Image reconstruction was performed using IDL (RSI Inc., Boulder, CO), subpixel volume registration using a C-language program (Thévenaz and Unser, 1998), and correlation processing and analysis was performed using Matlab (The Mathworks, Natick, MA). Cross-correlations were calculated for each pixel using an FFT approach for which low-frequency bins were attenuated to reduce influence of drift terms. Circular correlation with the full period m-sequence reference was performed, where the first 32 samples of transient were discarded at both the start of the run and the start of the inverse repeat (halfway into data). Correlation coefficients (versus time delay), $\rho(\tau)$, were calculated for each pixel by normalizing the correlation score $r_{xy}(\tau)$ by the standard deviation of the raw signal intensity fluctuation for each pixel. Estimate of the first off-diagonal elements of the second order kernel was $h_2(i,i-1) = \rho(i - 25)$, based on the specific m-sequence used (where the correlation waveform ρ is assumed to include the inverse repeat method). The above estimate ignores the fractional delay (between 0 and 1) in timing of image acquisition which varies for the eight slices acquired.

Mean correlation values for both first and second order response using the bullseye-gray paradigm were measured in the foveal and peripheral regions for nine volunteers. The foveal and peripheral regions were determined using the block paradigm by thresholding the t-scores that were generated by a regression analysis, which used a truncated
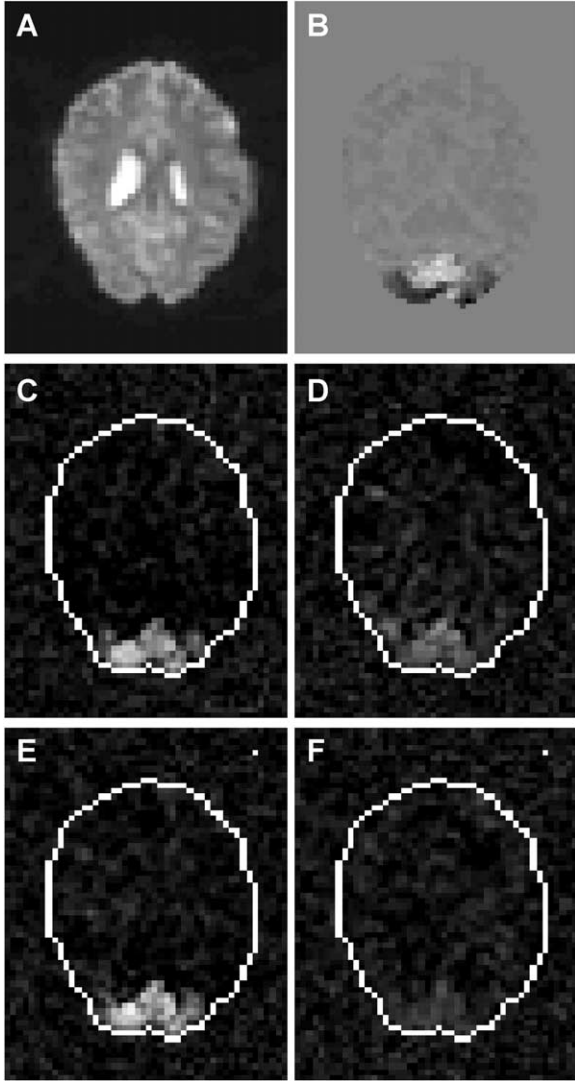
Fig. 5. Example fMRI images: (A) T2*-weighted signal intensity; (B) fovea-periphery *t*-score map; (C) and (D) first and second order response maps for bullseye-gray paradigm without gap, respectively; and (E) and (F) first and second order response maps for bullseye-gray paradigm with a 200-ms gap, respectively.

Gaussian ($\sigma = 3.5$ s) to model the hemodynamic response function. All image data were spatially registered for each experiment. Correlation scores were not temporally smoothed (matched filtered) for the hemodynamic response function; therefore the detection sensitivity is less than optimal.

Results

Fig. 5 shows example images using the bullseye-gray experimental paradigm. Fig. 5A is an intensity image for anatomical reference, and Fig. 5B is the *t*-score for the block design using the foveal bullseye and peripheral bullseye annulus. The foveal regions correspond to negative *t*-scores
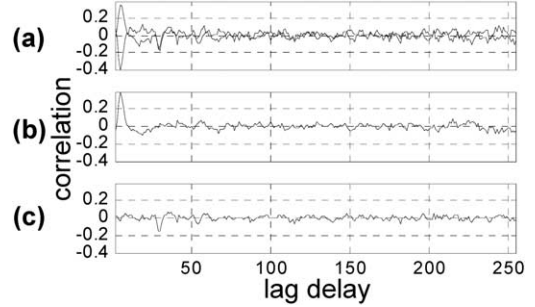

Fig. 6. Example correlation plots for pixel in foveal region using bullseye-gray paradigm: (a) raw correlation for inverse repeat; (b) odd order response (difference); and (c) even order response (sum).

(black) and the peripheral regions correspond to positive values (white). Correlation coefficient maps for the first (linear) and second (nonlinear) order responses are shown in Figs. 5C and D, respectively, using no gap between m-sequence stimuli. Correlation maps for the first and second order responses with a 200-ms gap between bits of the m-sequence are shown in Figs. 5E and F, respectively. The first order response is stronger in the foveal than peripheral region, while the second order response is stronger in the peripheral region. The second order response is greatly diminished using a gap of 200 ms (shown in Fig. 5F) as compared to no gap (shown in Fig. 5D). The second order response is displayed inverted, i.e., negative is bright, since the sign of h_2 is negative.

Example plots of the raw correlation waveforms from single pixels are shown in Figs. 6 and 7 to further illustrate the method and the relative strength of first and second order responses. The top plots are the superimposed raw correlation waveforms for normal and inverted polarity m-sequence stimulus probe to illustrate the inverse repeat method. The difference (center) and sum (bottom) correspond to odd and even order responses, respectively (scaled by 1/2 to reflect the average). Fig. 6 is from a pixel in the foveal region where the first order response is stronger. Fig. 7 is from a pixel in the peripheral region where the second order response is stronger. The first order response (estimate of linear hemodynamic response function) shows the characteristic undershoot following the main peak which is
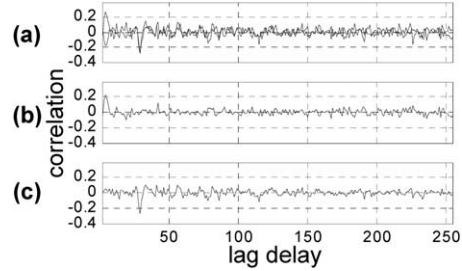

Fig. 7. Example correlation plots for pixel in peripheral region using bullseye-gray paradigm: (a) raw correlation for inverse repeat; (b) odd order response (difference); and (c) even order response (sum).
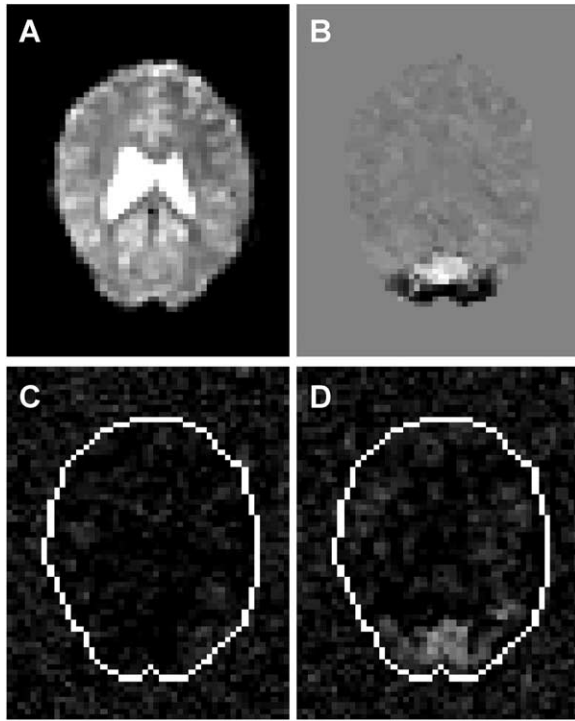
Fig. 8. Example fMRI images: (A) T2*-weighted signal intensity; (B) fovea-periphery *t*-score map; and (C) and (D) first and second order response maps for bullseye-reverse paradigm without gap, respectively.
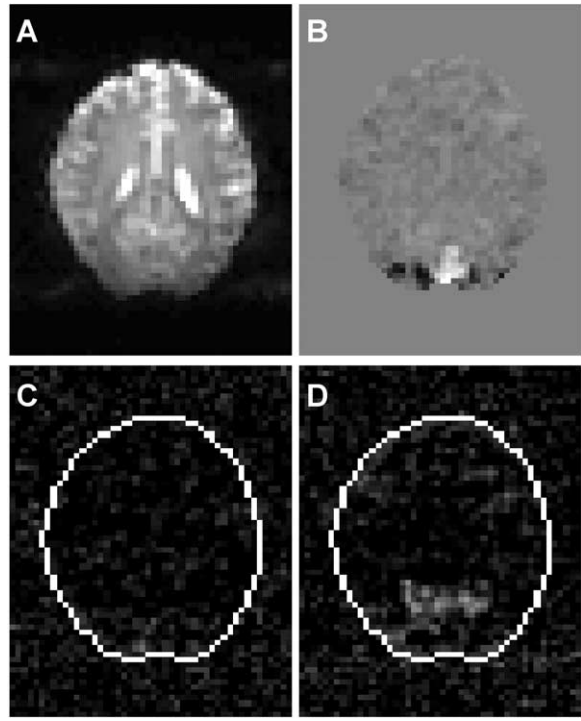

Fig. 9. Example fMRI images: (A) T2*-weighted signal intensity; (B) fovea-periphery *t*-score map; and (C) and (D) first and second order response maps for uniform disk paradigm without gap, respectively.

delayed approximately 3–4 s. Note that the second order response is delayed by 25 bits (s). There are no other stronger correlation responses at delays corresponding to other lag delays in the second order kernel, i.e., at 49 bits corresponding to $a_i \oplus a_{i-2}$ (see Discussion).

Figs. 8 and 9 show example images for bullseye-reversal and uniform disk-reversal (i.e., black and white) experimental paradigms (with no gap), respectively. Both cases exhibit no detectable linear response and significant second order response in the peripheral region. Fig. 10 plots the correlation waveform of a pixel in the peripheral region for the uniform disk case where the first order response is nondetectable, and the second order response is still fairly strong. Note that unlike for the bullseye, the correlation map for the disk has a significant response for the far periphery. This is due to the fact that a small amount of scattered light causes a temporal flicker in the magnet bore which stimulates the peripheral vision. The scattered light for the bullseye-reversal and bullseye-gray paradigms have constant mean luminance (after gamma correction), and, therefore, there is no temporal flicker to stimulate the periphery.

The mean correlation values using the bullseye-gray paradigm are graphed in Fig. 11 for nine experiments (seven volunteers). The first order response in the foveal region is generally stronger than in the periphery ($P < 0.13$, paired *t* test) (Fig. 11a), while the second order response is generally stronger in the peripheral region ($P < 0.005$) (Fig. 11b). The mean correlation values for the second order response in the

peripheral region is shown in Fig. 11c comparing data acquired with no gap and with a 200-ms gap (note that only seven datasets used both paradigms). The second order response is greatly reduced using a gap of 200 ms ($P < 0.002$).

Discussion

General remarks

The estimation efficiency of the hemodynamic response using the m-sequence probe method has been shown to be
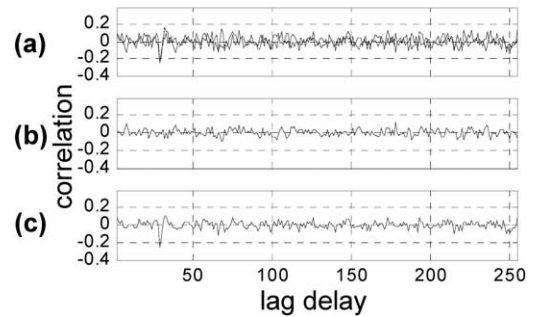

Fig. 10. Example correlation plots for pixel in peripheral region using uniform disk paradigm: (a) raw correlation for inverse repeat; (b) odd order response (difference); and (c) even order response (sum).
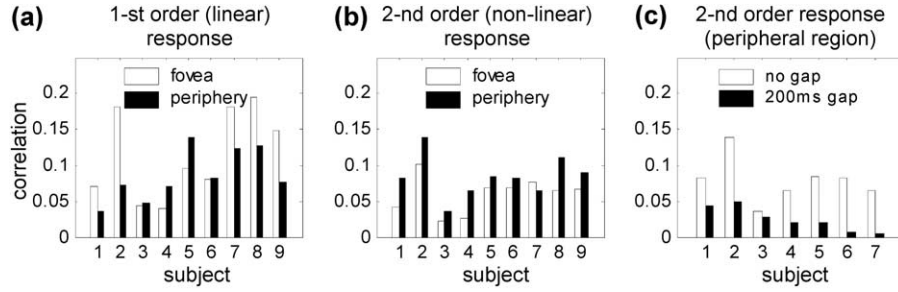
Fig. 11. Mean correlation scores for (a) first order (linear) response in fovea and periphery; (b) second order (nonlinear) response in fovea and periphery; and (c) second order response in periphery with and without gap.

near the achievable limit for event-related paradigms (Buracas and Boynton, 2002). The detection power of the first and second order response maps was degraded by two factors. The lowpass filter hemodynamic response reduced the correlation amplitude since a base period of 1 s was used for the m-sequence probe. Furthermore, temporal smoothing (matched filtering) was not used. The 1-s base period was chosen purposefully to oversample the hemodynamic response in order to test the hypothesis that the second order response was predominantly neuronal (i.e., single strong off-diagonal kernel coefficient). Temporal smoothing of the correlation waveform using an estimate of the kernel may be employed to reduce noise fluctuation. However, the kernel exhibited significant variations between subjects as well as across activated pixels within a subject. Several adaptive methods were tested which were found to improve the detectability for cases which were already reasonably good, but which were insufficiently robust to apply in all cases. The detection sensitivity of the block paradigm used to identify foveal and peripheral regions was significantly better than the m-sequence correlation maps; thus the threshold maps used to mask correlation scores shown in Fig. 11 included low signal-to-noise ratio pixels.

Significant gains can be made by means of basis fitting approaches using regression methods (Friston et al., 1998; Marmarelis, 1993); however, these approaches were specifically avoided to prevent incorrect model assumptions. In particular, while the hemodynamic response function is sufficiently sampled, the neuronal response is under sampled. The basis fitting method using Laguerre polynomial (Marmarelis, 1993) and gamma density (Friston et al., 1998) functions was tested. Basis fitting using a set of orthonormal Laguerre polynomials showed no improvement in the second order kernel estimate since it is insufficiently sampled. Basis fitting using a set of gamma density functions (Friston et al., 1998) provided an incorrect model fit which overestimated the contribution of off-diagonal terms. The correlation method does not make any model assumptions, although the correlation values must be interpreted. A benefit of calculating the complete correlation waveform (all delays across full period) is the ability to observe the presence of higher order nonlinearities based on detecting

additional anomalous peaks, which arise from the algebraic structure of the m-sequence.

Interpretation of results

The first issue of interpretation is whether the observed second order nonlinear response is due to the inherent nonlinearities of the visual system, to the BOLD response, or possibly to a mixture of effects. The contention is that the observed nonlinearity is predominantly neuronal in origin since the second order response largely disappears, using decorrelating delays on the order of hundreds of ms, which are long with respect to temporal dynamics associated with neurons, yet shorter than the hemodynamic response. This implies that a significant fraction of the second order response is due to a "fast" system characteristic of neuronal responses. Limited detectability prevents sensitive measurement of the weaker responses. Nevertheless, it is presumed that if the second order response was predominantly BOLD, the response $h_2(i, i–j)$ would be reasonably strong for several off-diagonal values of delay j based on the presumed Wiener model (LN cascade) for the BOLD effect where the linear system (L_2) has a response duration of several seconds (purposefully oversampled). In the case of the bullseye-reversal paradigm with gap, there are no m-sequence components to create an observable second order response (see Fig. 2 model outputs); thus any hemodynamic response nonlinearity (N_2) would not cause a second order response. However, in the case of the bullseye-gray paradigm with gap, there is still an m-sequence component due to the proportional linear response of filter L_1 (see Fig. 3 model outputs); thus a hemodynamic response nonlinearity (N_2) could contribute to the second order response. The model nonlinearity (rectification) used for Fig. 3 did not contribute to the second order response since the input signal was mostly unipolar as a result of earlier rectification (by N_1). Other forms of nonlinearity (e.g., squarer) could lead to a second order contribution. Other sources of nonlinearity with longer duration temporal dynamics are feedback mechanisms involving the LGN and/or pupil, and intracortical adaptation. In a few instances, a response was discernible at $h_2(i, i$-2), possibly caused by nonlinearity of the hemody-

namic response. Nevertheless, these experiments show that the fast neuronal response is the predominant source of the second order response. Finally, the finding that the strength of the second order response increased in the peripheral region is more likely to be a characteristic of the visual system and not a BOLD effect. While previous literature (Glover, 1999; Vazquez and Noll, 1998; Friston et al., 1998; Birn et al., 2001) suggests that the observed nonlinear response is related to the BOLD hemodynamic response, these findings were unable to distinguish between neuronal and hemodynamic effects based on the data. Furthermore, these studies have been conducted with considerably longer duration stimuli.

Given the assertion that the second order response map is related to the visual response, modeling the complete retinocortical path is a complex subject. Emerson et al., (1989) developed a structured block model of a nonlinear system which was comprised of a cascade of LNL systems for the retina, LGN, and cortex. In this model, the retina and LGN were modeled as a parallel cascade of "on" and "off" cells which were recombined by summation at the cortical input for a simple cell. In this way, the cortex was presented with the equivalent of a linear system input, since effects of the nonlinearities for "on" and "off" channels were balanced. The fMRI observations of the cortex were insufficient to validate this hypothesis; however, it might be possible to perform functional imaging of the LGN and/or retina with m-sequence probing to estimate first and second order responses which might help disentangle the complex cascade.

Preliminary findings are that the peripheral visual system has greater sensitivity to temporal contrast than the foveal region. Fig. 9D indicates that even a small percentage of bore flicker stimulates the peripheral vision with change in luminance (temporal contrast). Differences in the sensitivity and temporal characteristics of M- and P-cells, associated with peripheral and foveal regions, respectively, have been observed (in Macaque) (Derrington and Lennie, 1984). Baseler and Sutter (1997) have reported measured differences (in humans) in the amplitude of second order responses between P- and M-pathways using surface electrode recordings of visual evoked potential (VEP). The data in Fig. 11 depend on the specific eccentricity used for foveal vs peripheral stimulation (block paradigm), and may exhibit a more significant difference for a smaller foveal region.

Conclusions

Mapping of nonlinear response using fMRI provides a new method with potential for exploring neuronal responses and interactions. This method was demonstrated by mapping the primary visual system response. Probing of other areas may help further identify the system model. Refinement of this method for increased detection efficiency is being investigated.

Acknowledgments

References

Bandettini, P.A., Jesmanowicz, A., Wong, E.C., Hyde, J.S., 1993. Processing strategies for time-course data sets in functional MRI of the human brain. Magn. Reson. Med. 30, 161–173.

Baseler, H.A., Sutter, E.E., 1997. M and P components of the VEP and their visual field distribution. Vis. Res. 37, 675–690.

Benardete, E.A., Kaplan, E., 1997. The receptive field of the primate P retinal ganglion cell. II. Nonlinear dynamics. Vis. Neurosci. 14, 187–205.

Benardete, E.A., Victor, J.D., 1994. An extension of the m-sequence technique for the analysis of multi-input nonlinear systems, in: Marmarelis, V.Z. (Ed.), Advanced Methods of Physiological System Modeling, Vol. III, Plenum, New York, pp. 87–110.

Billings, S.A., 1980. Identification of nonlinear systems—A survey. IEE Proc. 127, 272–285.

Birn, R.M., Saad, Z.S., Bandettini, P.A., 2001. Spatial heterogeneity of the nonlinear dynamics in the FMRI BOLD response. NeuroImage 14, 817–826.

Boynton, G.M., Engel, S.A., Glover, G.H., Heeger, D.J., 1996. Linear systems analysis of functional magnetic resonance imaging in human V1. J. Neurosci. 16, 4207–4221.

Buracas, G.T., Boynton, G.M., 2002. Efficient design of event-related fMRI experiments using m-sequences. NeuroImage 16, 801–813.

Buxton, R.B., Wong, E.C., Frank, L.R., 1998. Dynamics of blood flow and oxygenation changes during brain activation: the balloon model. Magn. Reson. Med. 39, 855–864.

Derrington, A.M., Lennie, P., 1984. Spatial and temporal contrast sensitivities of neurones in lateral geniculate nucleus of Macaque. J. Physiol. 357, 219–240.

Emerson, R.C., Korenberg, M.J., Citron, M.C., 1989. Identification of intensive nonlinearities in cascade models of visual cortex and its relation to cell classification, in: Marmarelis, V.Z. (Ed.), Advanced Methods of Physiological System Modeling, Vol. II, Plenum, New York, pp. 97–111.

Friston, K.J., Jezzard, P., Turner, R., 1994. Analysis of functional MRI time series. Hum. Brain Mapp. 1, 153–171.

Friston, K.J., Josephs, O., Rees, G., Turner, R., 1998. Nonlinear event-related responses in fMRI. Magn. Reson. Med. 39, 41–52.

Friston, K.J., Mechelli, A., Turner, R., Price, C.J., 2000. Nonlinear responses in fMRI: the balloon model, Volterra kernels, and other hemodynamics. NeuroImage 12, 466–477.

Glover, G.H., 1999. Deconvolution of impulse response in event-related BOLD fMRI. NeuroImage 9, 416–429.

Golomb, S.W., 1968. Shift Register Sequences. Holden-Day, San Francisco.

Horton, J.C., Hoyt, W.F., 1991. The representation of the visual field in human striate cortex. A revision of the classic Holmes map. Arch. Ophthalmol. 109, 816–824.

Lee, Y.W., Schetzen, M., 1965. Measurement of the Wiener kernels of a non-linear system by cross-correlation. Int. J. Control 2, 237–254.

Marmarelis, P.Z., Marmarelis, V.Z., 1978. Analysis of Physiological Systems—The White Noise Approach. Plenum, New York.

Marmarelis, V.Z., 1993. Identification of nonlinear biological systems using Laguerre expansions of kernels. Ann. Biomed. Eng. 21, 573–589.

Miller, K.L., Luh, W.M., Liu, T.T., Martinez, A., Obata, T., Wong, E.C., Frank, L.R., Buxton, R.B., 2001. Nonlinear temporal dynamics of the cerebral blood flow response. Hum. Brain Mapp. 13, 1–12.

Ogawa, S., Lee, T.M., Stepnoski, R., Chen, W., Zhu, X.H., Ugurbil, K., 2000. An approach to probe some neural systems interaction by functional MRI at neural time scale down to milliseconds. Proc. Natl. Acad. Sci. USA 97, 11026–11031.

Reid, R.C., Victor, J.D., Shapley, R.M., 1997. The use of m-sequences in the analysis of visual neurons: linear receptive field properties. Vis. Neurosci. 14 , 1015–1027.

Schetzen, M., 1980. The Volterra and Wiener Theories of Nonlinear Systems. Wiley, New York.

Sutter, E.E., 1987. A practical nonstochastic approach to nonlinear time-domain analysis, in: Marmarelis, V.Z. (Ed.), Advanced Methods of Physiological System Modeling, Vol. 1, Plenum, New York, pp. 303–315.

Sutter, E.E., 2001. Imaging visual function with the multifocal m-sequence technique. Vis. Res. 41, 1241–1255.

Thévenaz, P., Unser, M., 1998. A pyramid approach to subpixel registration based on intensity. IEEE Trans. Image Proc. 7, 27–41.

Vazquez, M.L., Noll, D.C., 1998. Nonlinear aspects of the BOLD response in functional MRI. NeuroImage 7, 108–118.

Wiener, N., 1958. Nonlinear Problems in Random Theory. The Technology Press of MIT and Wiley, New York.